JOURNAL OF
THE
INDIAN INSTITUTE OF SCIENCE
SECTION B

VOLUME 39 OCTOBER 1957 NUMBER 4

SOME INVESTIGATIONS ON DIELECTRIC AERIALS—PART III

By B. Rama Rao, (Mrs.) R. Chatterjee and S. K. Chatterjee
(*Department of Electrical Communication Engineering, Indian Institute of Science, Bangalore-3*)

Received July 20, 1957

Abstract

The two theories (Chatterjee *et al.*, 1956, 1957) for the radiation of a dielectric rod aerial excited in the HE_{11} mode have been experimentally verified in the case of perspex rod aerials of lengths varying from $2\lambda_0$ to $10\lambda_0$ and diameter $0{\cdot}5\lambda_0$ in the $\Phi = 0°$ plane. Experiments have also been done for aerials of different diameters varying from $0{\cdot}4\lambda_0$ to $0{\cdot}8\lambda_0$ and length $10\lambda_0$.

There is close agreement between the two theories and experiment with regard to the positions of maxima and minima for the higher order secondary lobes. In the case of the first minor lobe for some values of L/λ_0 the deviation is appreciable. Measured values of beam width for major lobes for different lengths of aerial and $d = 0{\cdot}5\lambda_0$ agree fairly well with the theoretical values.

Introduction

The paper presents a report of the experimental verification in the $\Phi = 0°$ plane of the theories (*loc. cit.*) for the radiation characteristics of a dielectric rod aerial excited in the HE_{11} mode in the X-band ($\lambda_0 = 3{\cdot}2$ cm.). A comparative study is made between the positions of maxima and minima of the lobes, as obtained by experiment and the two theories (1956, 1957) based on Schelkunoff's Equivalence principle and Huyghen's principle.

Theoretical

The radiation field intensity at any distant point P in the $\Phi = 0°$ plane as derived by using Schelkunoff's Equivalence principle is (Chatterjee *et al.*, 1956)

$$\vec{E}_p = \vec{u}_\Phi \omega\mu_0 K_1^{H} \left[\frac{\sin\{(\beta - k\cos\theta)\,L\}}{(\beta - k\cos\theta)}\right] 2\pi J_1\left(\frac{kd}{2}\sin\theta\right)$$

$$+ \vec{u}_\theta k K_1^{E} \left[\frac{\cos\{(\beta - k\cos\theta)\,L\} - 1}{(\beta - k\cos\theta)}\right] \frac{2\sqrt{2\pi}}{\left(\frac{kd}{2}\sin\theta\right)^{\frac{1}{2}}}$$

$$\times J_{\frac{1}{2}}\left(\frac{kd}{2}\sin\theta\right) \qquad (1)$$

whereas, the radiation field intensity at P in the $\Phi = 0°$ plane derived on the basis of Huyghen's principle is (Chatterjee *et al.*, 1957)

$$E_p \propto \left\{J_0\left(\frac{kd}{2}\sin\theta\right) + J_2\left(\frac{kd}{2}\sin\theta\right)\right\} \frac{\sin\left\{\frac{L}{2}(\beta - k\cos\theta)\right\}}{\frac{L}{2}(\beta - k\cos\theta)} \qquad (2)$$

The values of x_1 and x_2 involved in K_1^{H} and K_1^{E} have been calculated by solving the following equations (Chatterjee *et al.*, *loc. cit*).

$$\left[\frac{1}{x_1}\frac{J_1'(x_1)}{J_1(x_1)} - \frac{1}{x_2}\frac{H_1'(x_2)}{H_1(x_2)}\right]\left[\frac{\bar{\epsilon}_1}{x_1}\frac{J_1'(x_1)}{J_1(x_1)} - \frac{1}{x_2}\frac{H_1'(x_2)}{H_1(x_2)}\right]$$

$$= \frac{(x_1^2 - x_2^2)(x_1^2 - x_2^2\,\bar{\epsilon}_1)}{x_1^4\,x_2^4} \qquad (3)$$

and

$$x_1^2 + \left(\frac{x_2}{j}\right)^2 = \left(\frac{\pi d}{\lambda_0}\right)^2 (\bar{\epsilon}_1 - 1) \qquad (4)$$

The graphical solution for Equation (3) for a perspex rod of $d = 0{\cdot}5\,\lambda_0$ and $\bar{\epsilon}_1 = 2{\cdot}62$ is given in Fig. 1. The values of x_1 and x_2 obtained from Fig. 1 are $x_1 = 1{\cdot}714$ and $x_2 = j\,(1{\cdot}028)$ which yields the propagation constant of the mode $\gamma = j\,233{\cdot}17$.

EXPERIMENTAL

(i) *Excitation of dielectric aerial.*—The dielectric aerial is excited by means of a waveguide mode transformer (Fig. 2). The transformer consists of a rectangular guide which gradually transforms into a circular guide. The rectangular guide is excited by H_{10} mode and hence the circular guide is excited in the H_{11} mode. The dielectric aerial which is tightly fitted into the circular portion of the transformer by means of split collars is excited in the HE_{11} mode, in order that the boundary conditions may be satisfied on the dielectric surface. The portion of the dielectric aerial inside the circular guide is tapered in order to have proper matching with the guide. The photograph (Fig. 3) shows some of the dielectric aerials, split collars and the waveguide transformer fitted with a dielectric aerial.

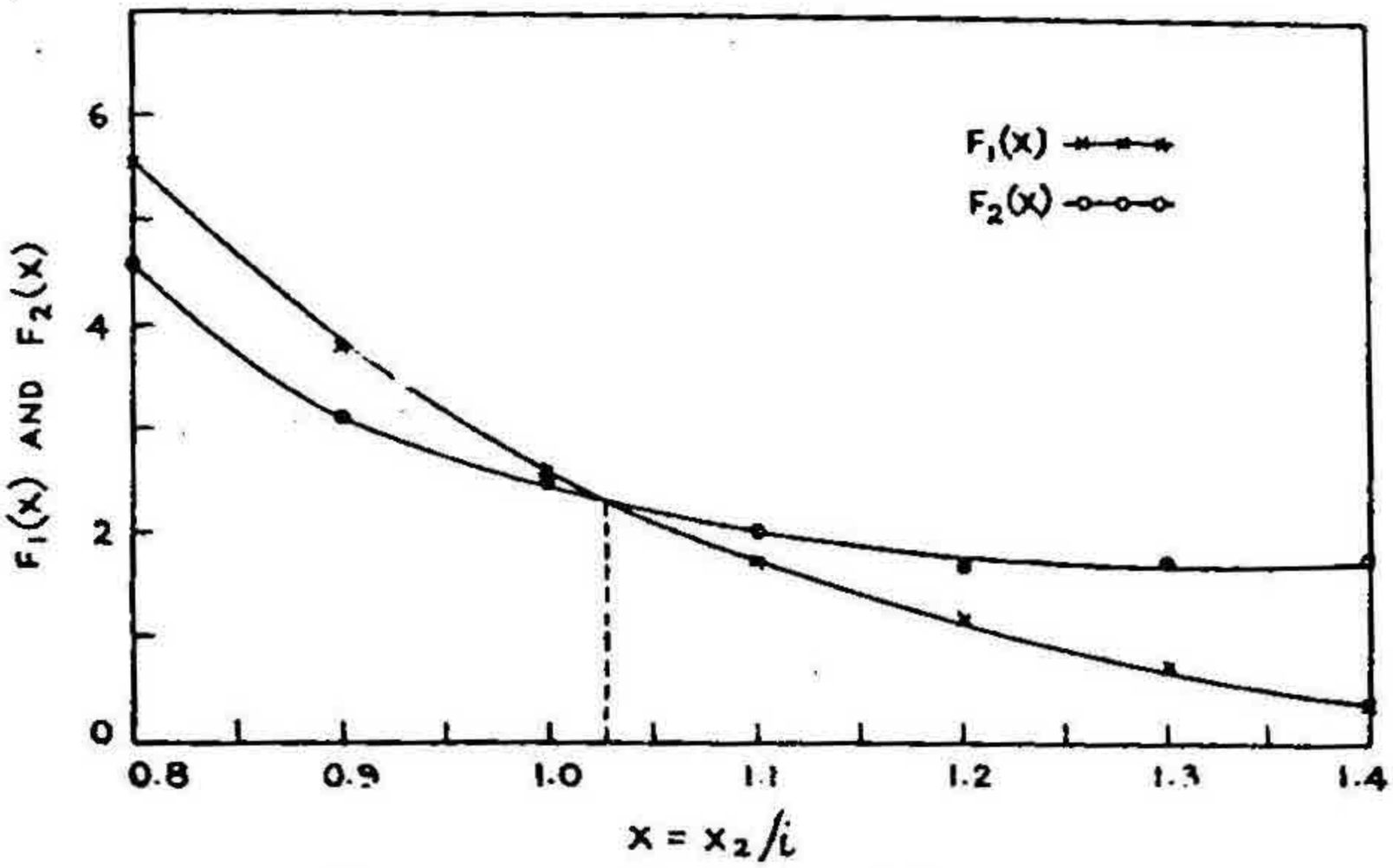

FIG. 1. Graphical solution of Equation 3.

$$F_1(x) = \left[\frac{1}{x_1} \cdot \frac{J_1'(x_1)}{J_1(x_1)} - \frac{1}{x_2} \cdot \frac{H_1'(x_2)}{H_1(x_2)}\right]\left[\frac{\bar{\epsilon}_1}{x_1} \cdot \frac{J_1'(x_1)}{J_1(x_1)} - \frac{1}{x_2} \cdot \frac{H_1'(x_2)}{H_1(x_2)}\right]$$

$$F_2(x) = \frac{(x_1^2 - x_2^2)\,(x_1^2 - x_2^2 \cdot \bar{\epsilon}_1}{x_1^4 \cdot x_2^4}$$

where

$$x_1^2 = \left(\frac{\pi d}{\lambda_0}\right)^2 (\bar{\epsilon}_1 - 1) \quad \text{and} \quad x_2 = ix.$$

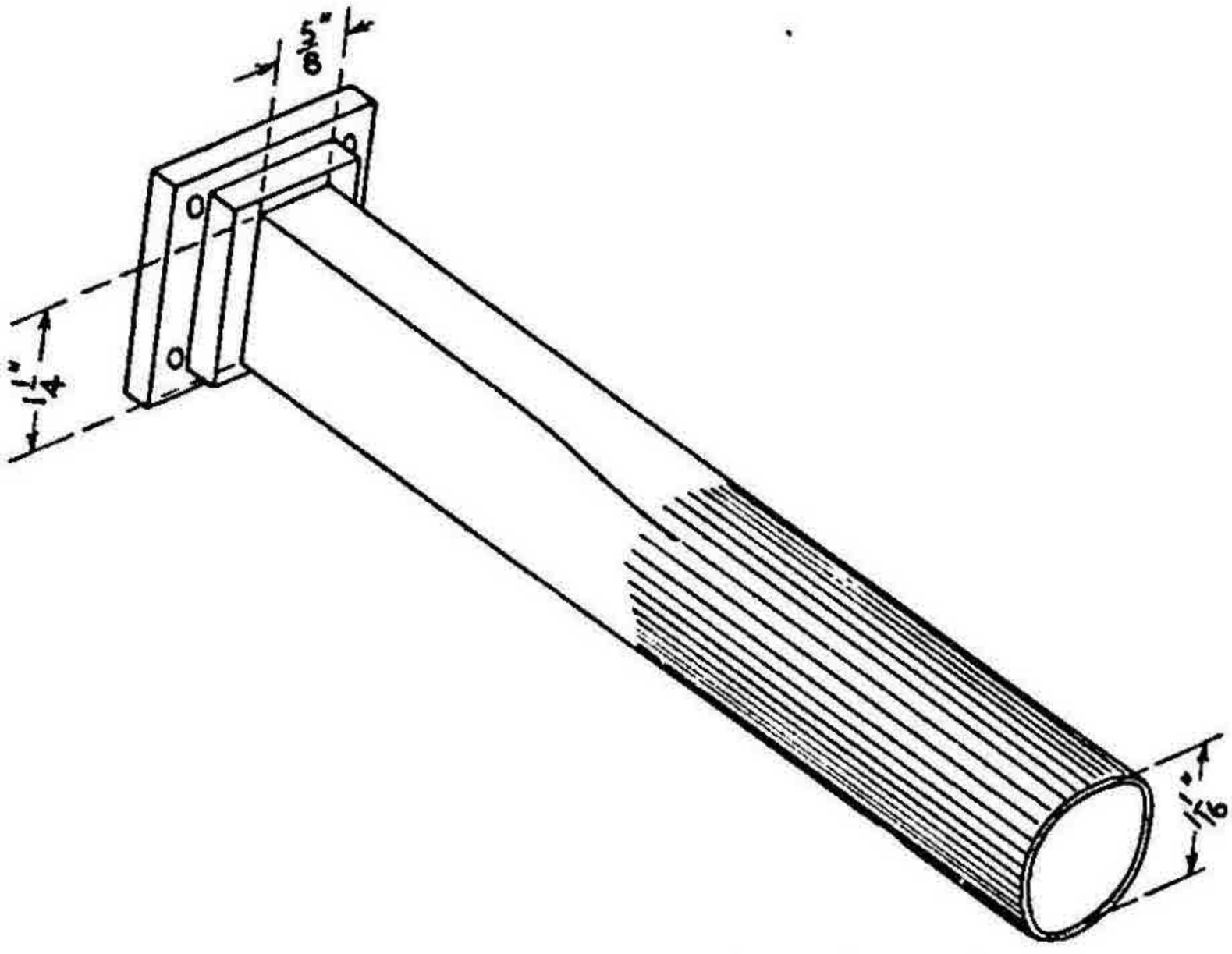

FIG. 2. Dimensioral sketch of the mode transformer.

(ii) *Pyramidal horn.*—A pyramidal horn excited by a 723 A/B klystron is used as a transmitting aerial. The dielectric rod is used as a receiving antenna. The dimensional sketch of the pyramidal horn is shown in Fig. 4. The radiation intensity pattern in the $\phi = 0°$ plane of the pyramidal horn is shown in Fig. 5. The measured gain of the horn is 18 db. as compared to the theoretical gain of 20 db.

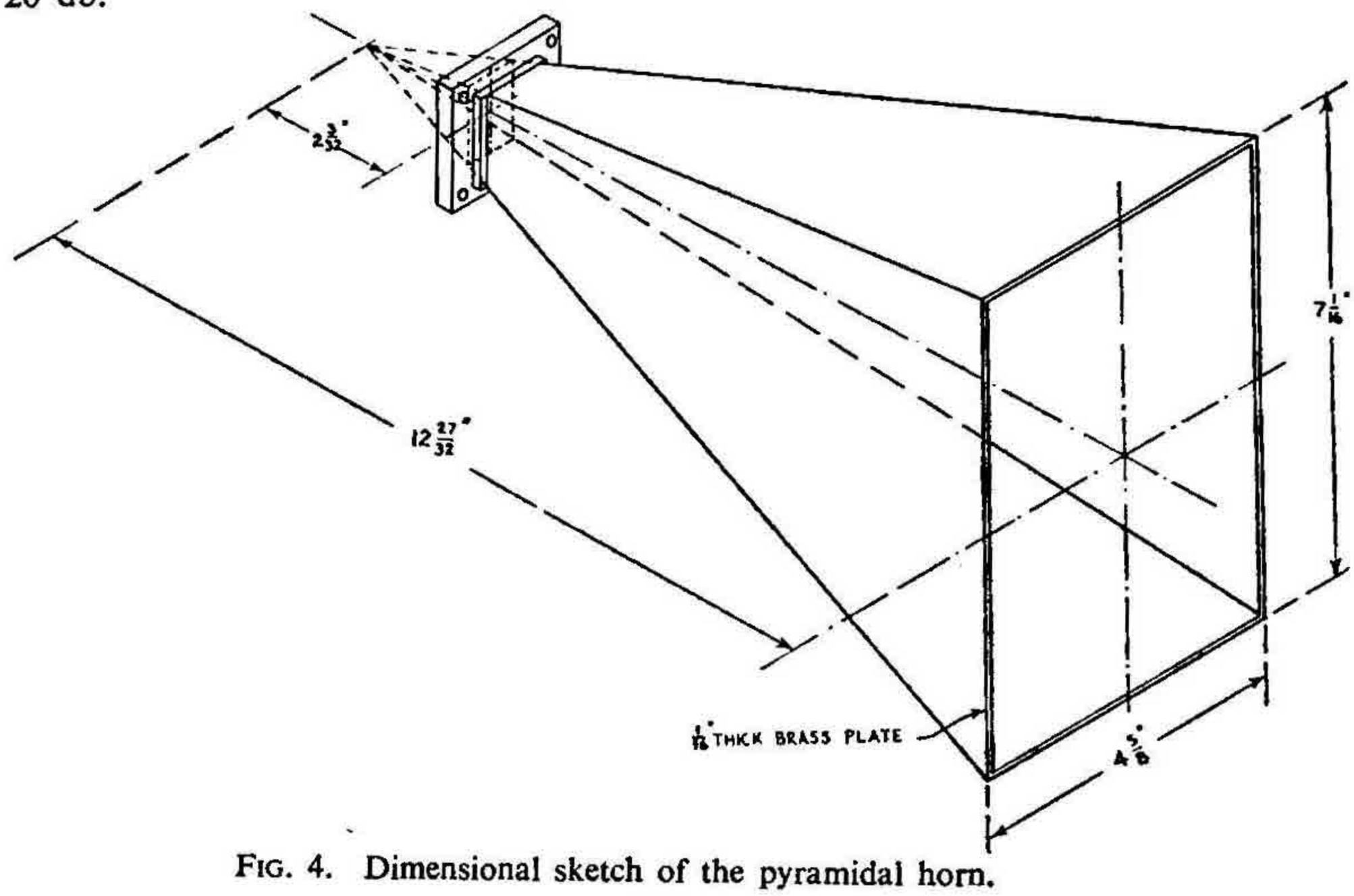

FIG. 4. Dimensional sketch of the pyramidal horn.

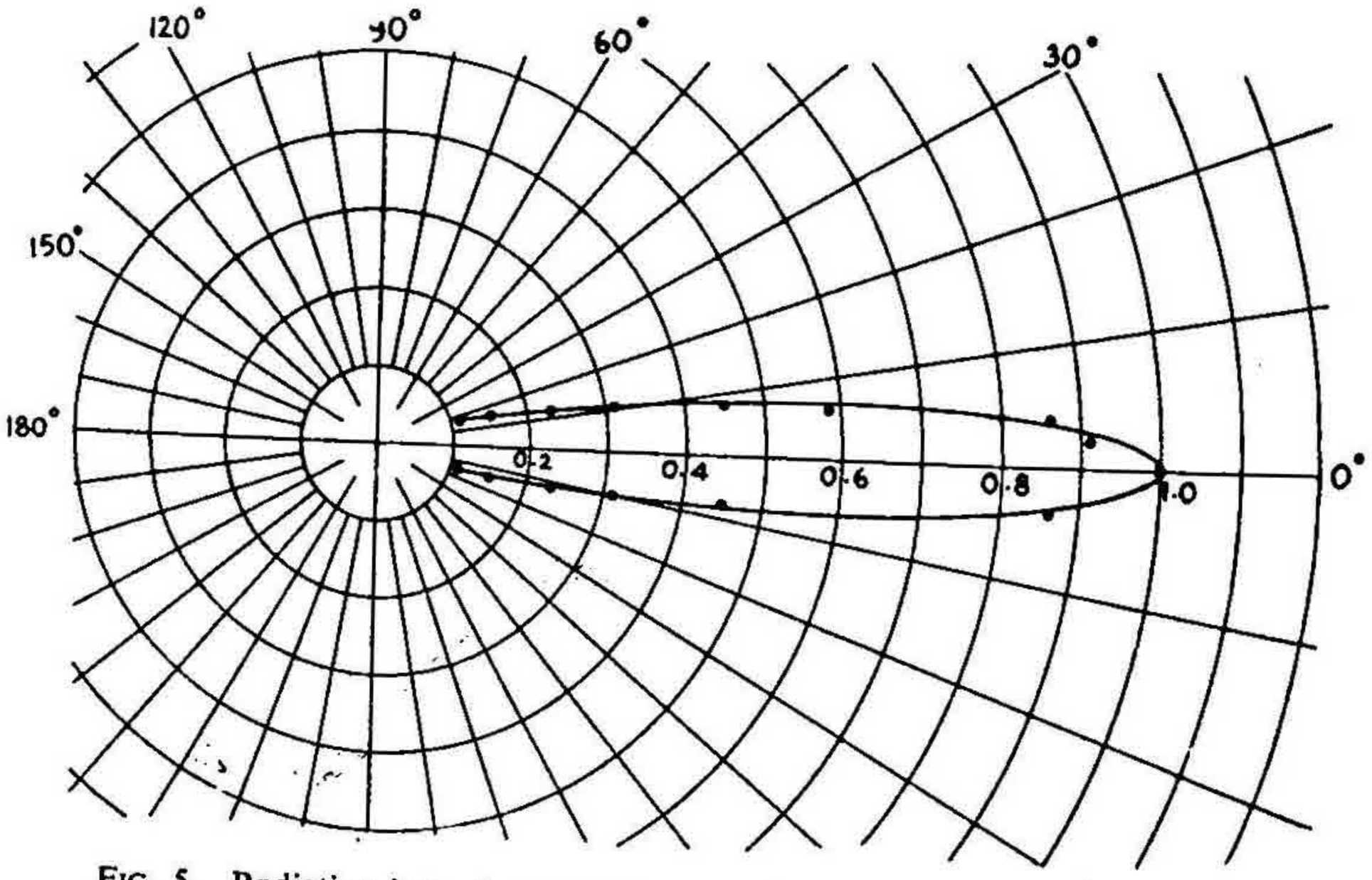

FIG. 5. Radiation intensity pattern in the $\Phi = 0°$ plane of the pyramidal horn.

(iii) *Mounting of the aerial.*—The aerial is mounted on a turntable graduated in degrees and supported at a height of about 8 feet from the ground by means of tripod stand. The turntable can be rotated smoothly and the angle read by means of a pointer attached to the stand.

(iv) *Power supply.*—The pyramidal horn is excited by a reflex klystron 723 A/B which is fed by an electronically regulated power supply unit. The characteristics of the power supply unit have been reported elsewhere (Chatterjee *et al.*, 1955).

(v) *Detector.*—The waveguide transformer fitted with dielectric aerial at the circular end is attached to a detecting section at the rectangular end. The output of the crystal is fed into a twin-tee amplifier, the output of which is fed to a bridge network two arms of which consist of 1N34 crystal. The output from the bridge is fed to a microammeter. The characteristics of the detector amplifier have been reported elsewhere (Chatterjee *et al.*, 1954).

(vi) *Spacing of the aerial and horn.*—The emerging wavefront from the pyramidal horn is spherical. For correct measurements of aerial characteristics, it is necessary that the entire aperture of the test aerial be uniformly illuminated. This requires that the wave incident on the aperture of the test aerial possesses a plane wave front. In order to fulfil this condition, it is desirable to have as large a spacing as possible between the aerial and the horn. The minimum distance requirement that satisfies the Fraunhoffer zone characteristics is

$$\text{spacing} \geqslant \frac{2a^2}{\lambda_0} \tag{5}$$

where 'a' represents the aperture of the test aerial.

(vii) *Site.*—An open site for the experiment was chosen so as to avoid the effect of reflections on the radiation pattern from any nearby object. The effect of changing the frequency of the klystron on the radiation pattern was observed to be nil. This suggested that the effect of reflections, if any, was negligible.

(viii) *Open end radiation of the waveguide transformer.*—The radiation characteristics of the open end waveguide transformer was studied with and without the split collars attached. It was found that radiation could not be detected in the case of the mode transformer attached with only a collar made to fit aerials having $d \leq 0{\cdot}5\,\lambda_0$. But radiation could be detected in the case of the mode transformer attached with the collar made to fit aerials having $d > 0{\cdot}5\,\lambda_0$. The radiation characteristics of the mode transformer fitted with the collar made to fit the aerial having $d = 0{\cdot}6\,\lambda_0$ but without the aerial is shown in Fig. 6.

(ix) *Radiation pattern.*—Several radiation patterns of aerials were taken with different spacings between the transmitting and receiving aerials. One of the radiation intensity patterns taken at a spacing of 19 feet for a perspex rod of length $L = 3\,\lambda_0$ and diameter $d = 0.5\,\lambda_0$ is shown in Fig. 7. The wiggles on the lobes arise probably from the interaction between the aerial and the horn. The final radiation patterns were taken with a spacing of 50 feet which is approximately $470\,\lambda_0$.

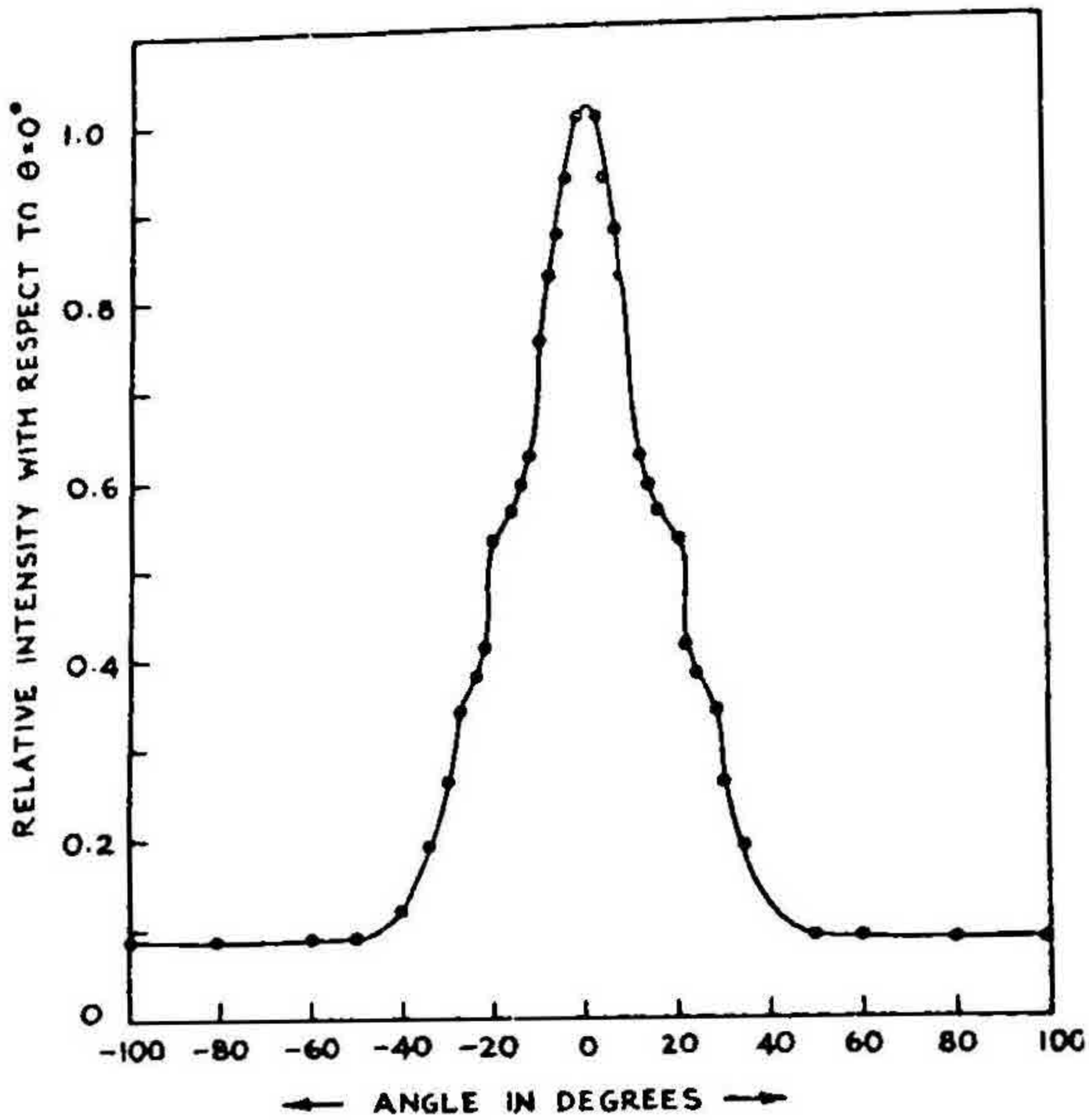

FIG. 6. Radiation intensity pattern in the $\Phi = 0°$ plane of a dielectric aerial, $d = 0{\cdot}5\,\lambda$, and $L = 3\,\lambda_0$ when the spacing between the aerial and the horn is 19 feet.

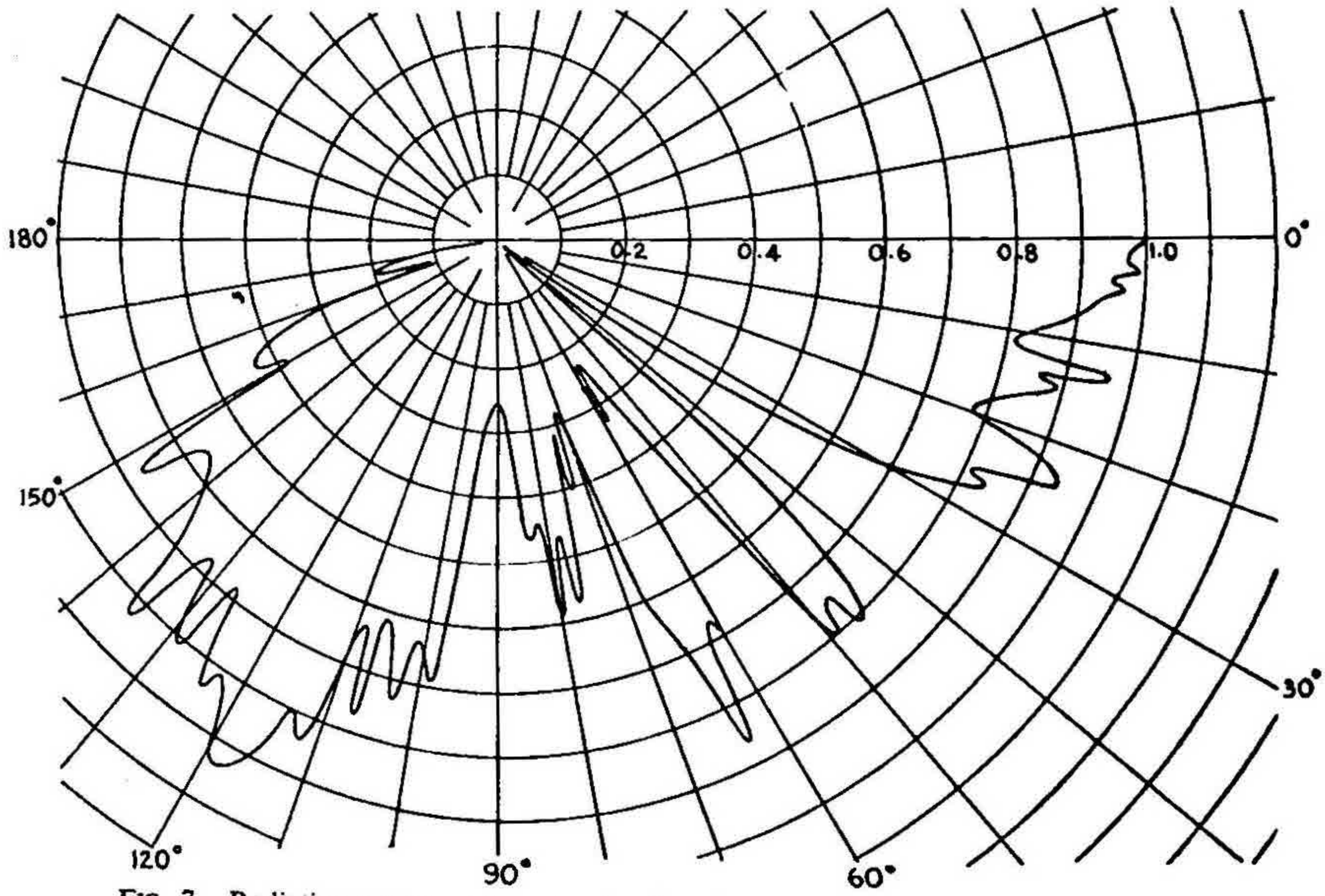

FIG. 7. Radiation power pattern in the $\Phi = 0°$ plane of the mode transformer attached with collar made to fit the aerial having $d = 0{\cdot}6\,\lambda_0$.

Experiments were done with aerials having $d = 0{\cdot}5\,\lambda_0$ and lengths varying from $2\lambda_0$ to $10\,\lambda_0$. Experiments were also done with aerials having length $L = 10\,\lambda_0$ and diameters varying from $0{\cdot}4\,\lambda_0$ to $0{\cdot}8\,\lambda_0$. The radiation patterns for $L = 2\,\lambda_0$ and $d = 0{\cdot}5\,\lambda_0$ are presented in Figs. 8 and 9. The dotted curves in both the

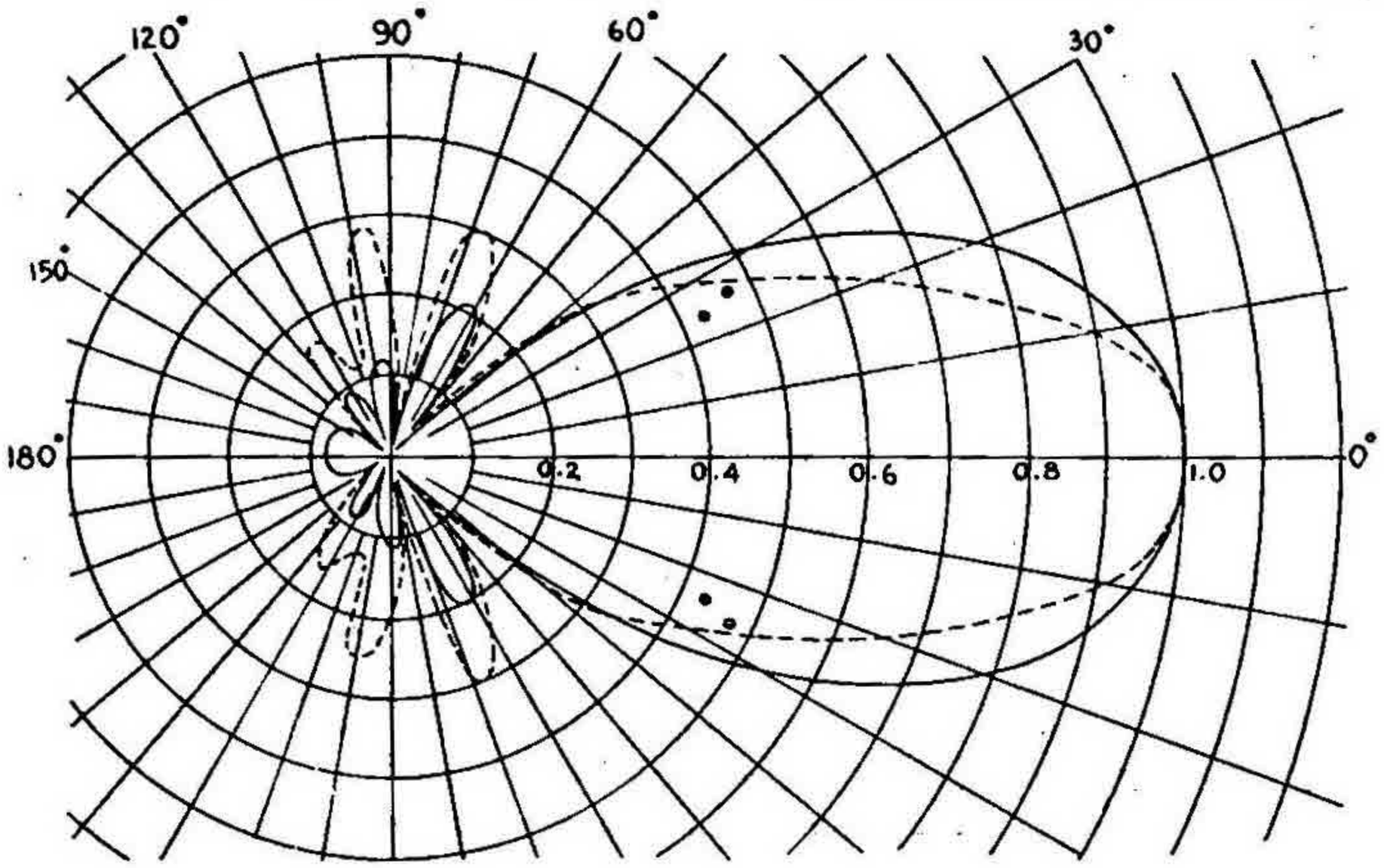

FIG. 8. Theoretical (Equation 1) and experimental radiation intensity patterns for a perspex rod of $L = 2\,\lambda_0$, $d = 0{\cdot}5\,\lambda_0$, $\epsilon_1 = 2{\cdot}62$. —— Theoretical (Schelkunoff's Equivalence principle); --- Experimental.

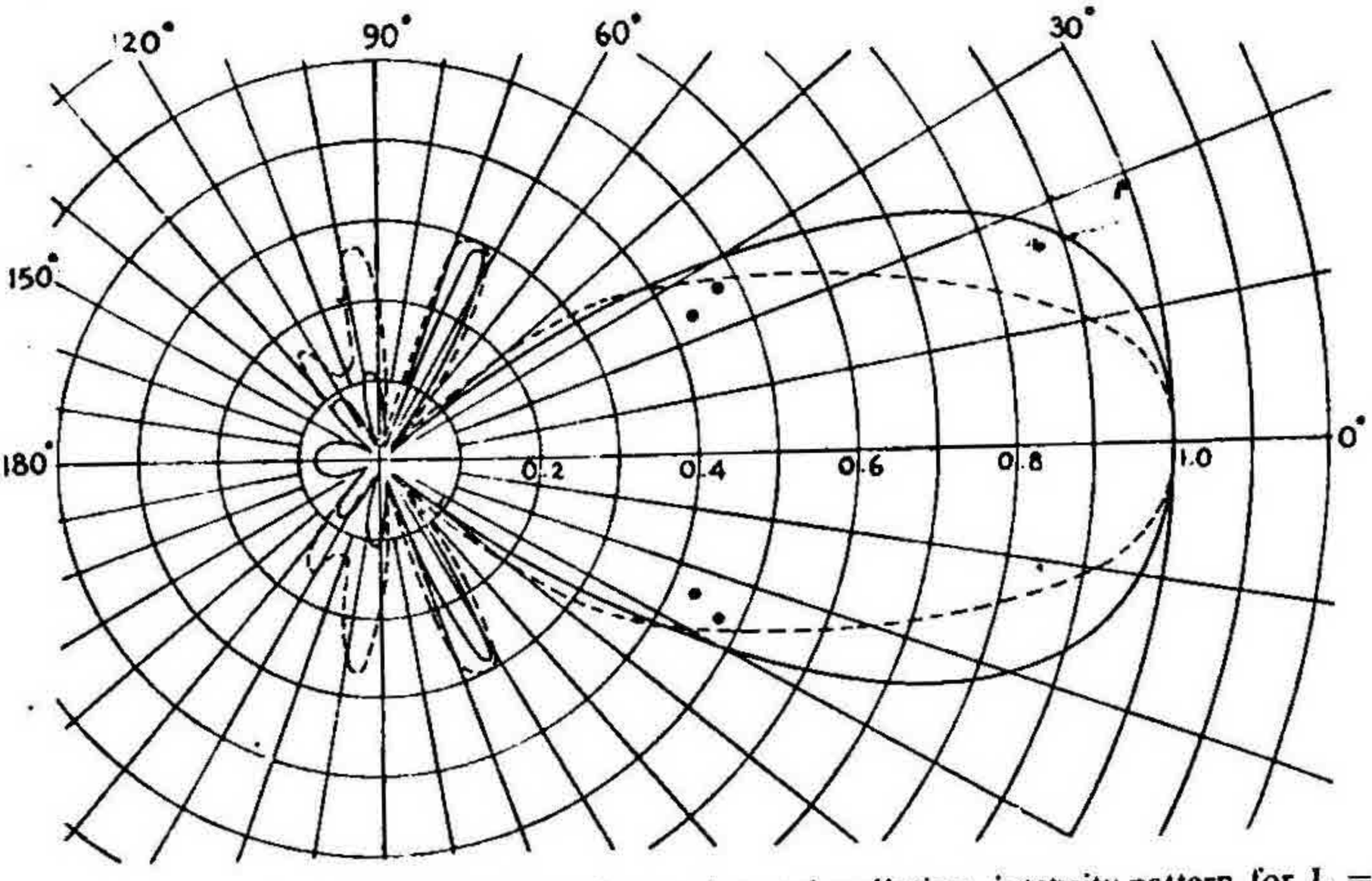

FIG. 9. Theoretical (Equation 2) and experimental radiation intensity pattern for $L = 2\,\lambda_0$, $= 0{\cdot}5\,\lambda_0$, $\epsilon_1 = 2{\cdot}62$. —— Theoretical (Huyghen's principle); --- pxperimental.

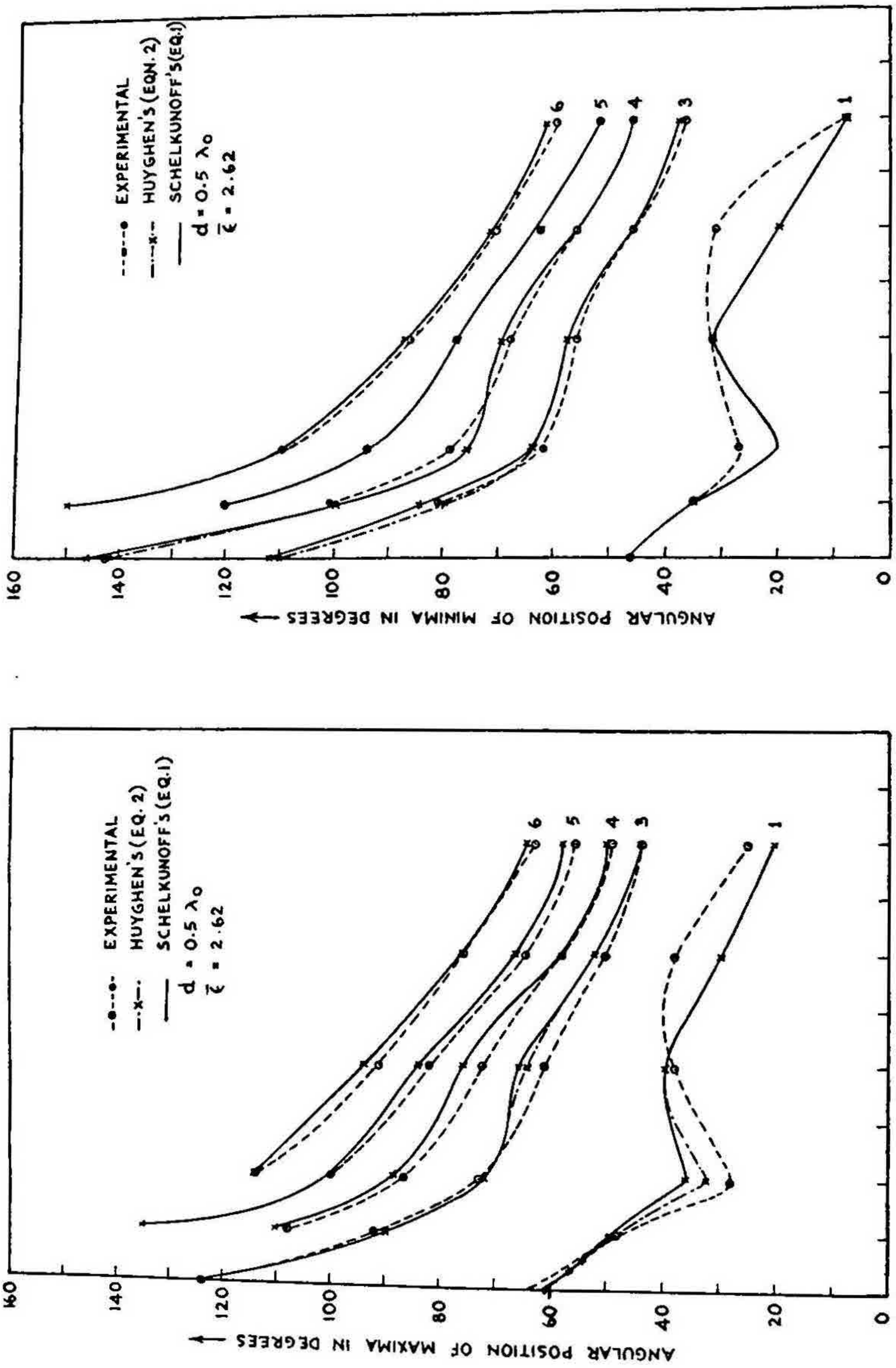

FIG. 11. Theoretical and experimental positions of minima varying with L/λ_0, $d/\lambda_0 = 0{\cdot}5$, $\bar{\epsilon}_1 = 2{\cdot}62$.

FIG. 10. Angular positions of side lobes varying with L/λ_0 for $d = 0{\cdot}5\ \lambda_0$ and $\bar{\epsilon}_1 = 2{\cdot}62$.

figures represent the experimental results. The solid curves represent theoretical results calculated from Schelkunoff's Equivalence principle (Equation 1) and extended Huyghen's principle (Equation 2) respectively. The four small circles in the above figures are experimental points.

Discussion

(i) The positions of maxima of some of the minor lobes for rods of $d = 0{\cdot}5\ \lambda_0$ and $\bar{\epsilon}_1 = 2{\cdot}62$ are represented in Fig. 10. It is found that there is close agreement between experiment and the two theories for the higher order secondary lobes. There is however some appreciable difference for some values of L/λ_0 in the case of the first minor lobe. Data for the second lobe have not beeen plotted for lack of .larity of the figure. This agreement is also noticed for secondary lobes higher than the sixth in the case of aerials of lengths $6\ \lambda_0$, $8\ \lambda_0$ and $10\ \lambda_0$ as shown in Table I.

TABLE I

Positions of maxima of secondary lobes higher than the sixth

Lobes	$6\ \lambda_0$			$8\ \lambda_0$			$10\ \lambda_0$		
	Theory Eq. 1	Theory Eq. 2	Expl.	Theory Eq. 1	Theory Eq. 2	Expl.	Theory Eq. 1	Theory Eq. 2	Expl.
7	104°	104°	100°	82°	82°	82°	70°	70°	69°
8	114	114	112	90	90	89	76	76	75
9	124	124	121	98	98	95	82	82	81
10	138	138	133	104	104	104	88	88	87
11				112	112	110	94	94	93
12				120	120	117	100	100	97
13				128	128	125	106	106	104
14				138	138	141	112	112	109
15							118	118	117

For aerials of lengths $2\ \lambda_0$, $3\ \lambda_0$, $4\ \lambda_0$, lobes higher than the sixth were not observed.

(ii) *Positions of minima of secondary lobes higher than the sixth.*—The variations of the positions of the minima with L/λ_0 and $d = 0{\cdot}5\ \lambda_0$ up to the sixth order secondary lobes are shown in Fig. 11. Data for the second minor lobe have been omitted for the reasons stated above. It is observed that the locations of minima

agree generally within $\pm$ 1° between the measured and the theoretical values except for the first minor lobe. There is also close agreement between the two theories and experimental positions of minima for the secondary lobes higher than the sixth as shown in Table II.

TABLE II

Positions of minima of secondary lobes higher than the sixth

Lobes	6 λ_0			8 λ_0			10 λ_0		
	Theory Eq. 1	Theory Eq. 2	Expl.	Theory Eq. 1	Theory Eq. 2	Expl.	Theory Eq. 1	Theory Eq. 2	Expl.
7	98°	98°	96°	78°	78°	78°	66°	66°	66°
8	110	110	106	88	88	85	72	72	72
9	118	118	116	94	94	92	78	78	78
10	130	130	127–130	100	100	98–100	84	84	84
11	146	146	144	110	110	106′	90	90	89
12		114	114	114	96	96	95		
13		124	124	123	102	102	101		
14		134	134	138	110	110	107		
15		142	142	144	114	114	113		
16		158	158	157					

(iii) *Positions and relative intensity of maximum intensity lobe.*—It is found that for some of the diameters, the intensity of some minor lobes becomes greater than that of the major lobe. The variation of the positions and relative intensities of such lobes with d/λ_0 is shown in Figs. 12 and 13 respectively. But it is found that for a rod of $d = 0{\cdot}5\ \lambda_0$, the major lobe intensity at $\theta = 0°$ is greater than that of any other lobe for lengths varying from $2\ \lambda_0$ to $10\ \lambda_0$. This is shown in Fig. 14.

(iv) *Positions of minor lobes varying with* d/λ_0.—The measured values of the maxima of minor lobes show an oscillatory variation with different d/λ_0 for $L = 10\lambda_0$ as indicated in Fig. 15. The theoretical variation with d/λ_0 will be reported in a later paper. It may be mentioned that in the absence of a theoretical curve, more importance should be attached to the positions of the individual points rather than to the lines joining them.

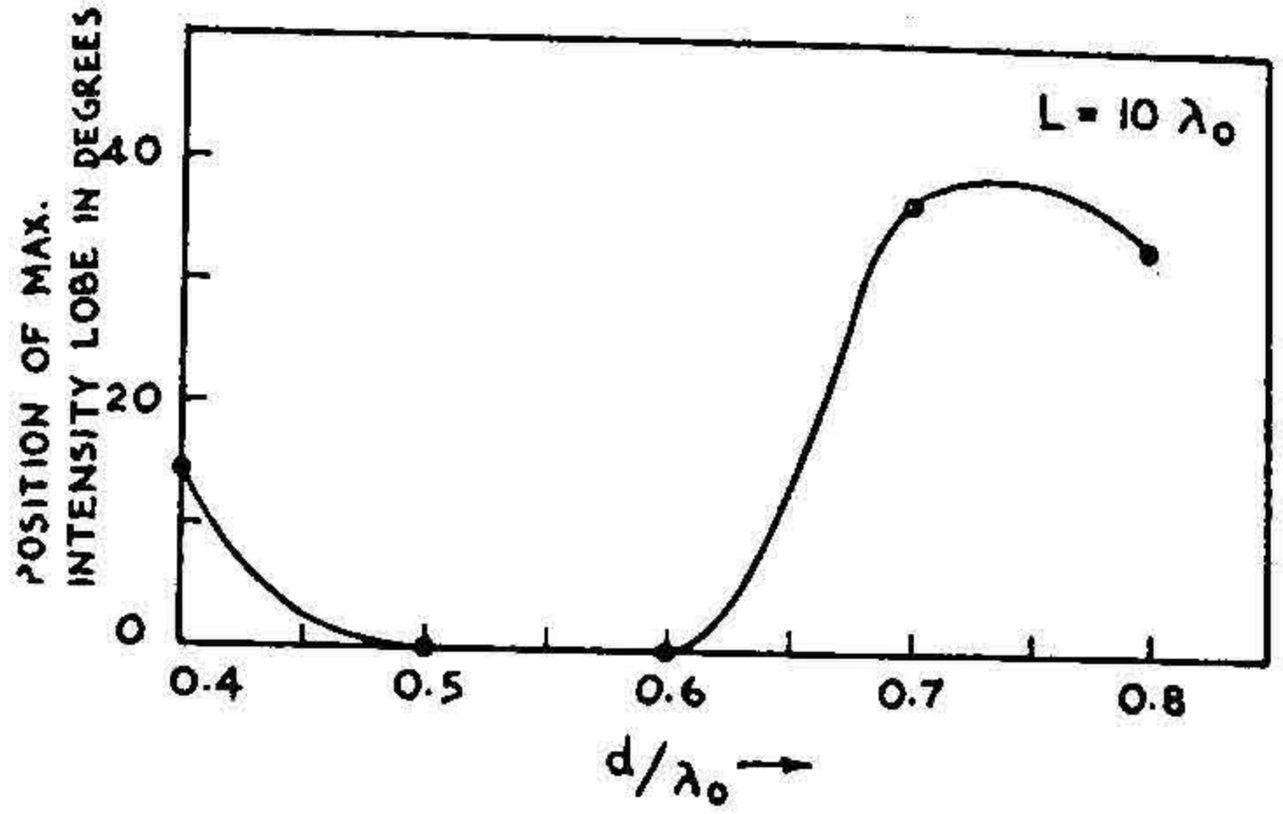

FIG. 12. Measured angular positions of maximum intensity lobe varying with d/λ_0 for $L = 10\lambda_0$ and $\tilde{\epsilon}_1 = 2{\cdot}62$.

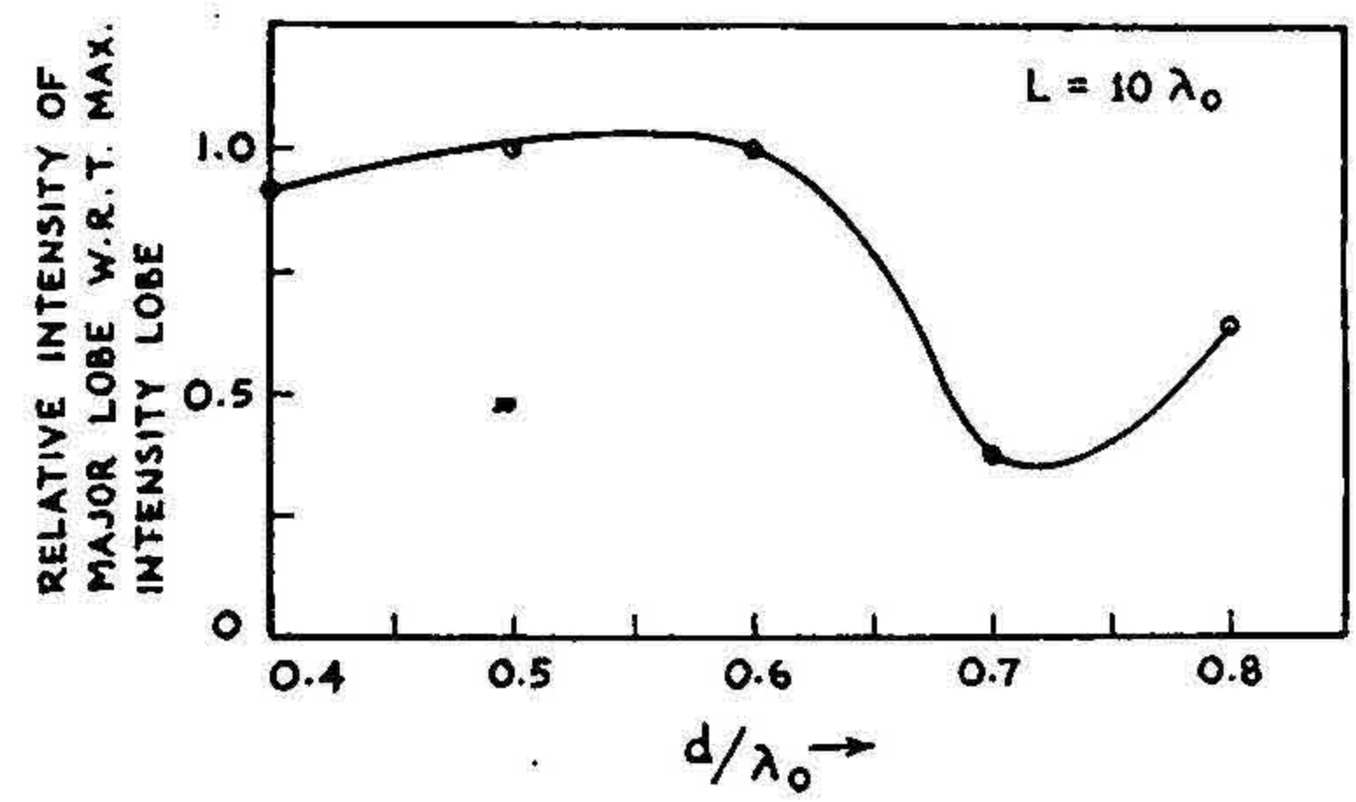

FIG. 13. Measured relative intensity of major lobe with respect to the maximum intensity lobe varying with d/λ_0 for $L = 10\lambda_0$ and $\tilde{\epsilon}_1 = 2{\cdot}62$.

FIG. 14. Positions of maximum intensity lobe varying with L/λ_0, $d = 0{\cdot}5\lambda_0$.

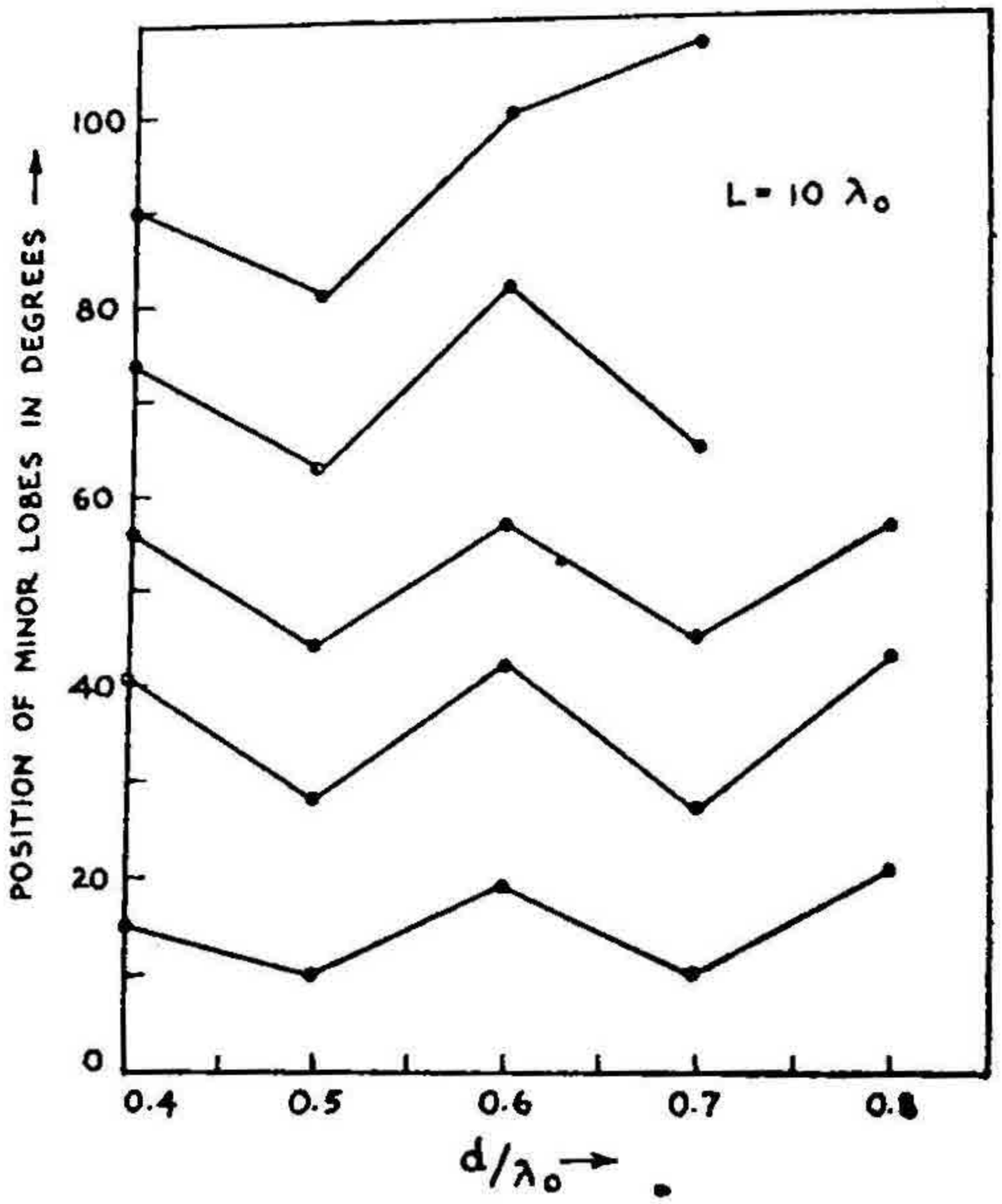

FIG. 15. Angular positions of minor lobes varying with d/λ_0 for $L = 10\,\lambda_0$.

(v) *Beam width.*—The beam width of the major lobes taken at 0·707 of the maxima for some of the aerials are reported in Table III.

TABLE III

Beam width of major lobe $d = 0{\cdot}5\,\lambda_0$, $\bar{\epsilon}_\perp = 2{\cdot}62$

Length	Experimental	Theoretical Equation 1	Theoretical Equation 2
$2\,\lambda_0$	39°	50°	48°
$3\,\lambda_0$	32°	34°	36°
$8\,\lambda_0$	21°	22°	24°

Further work is under progress.

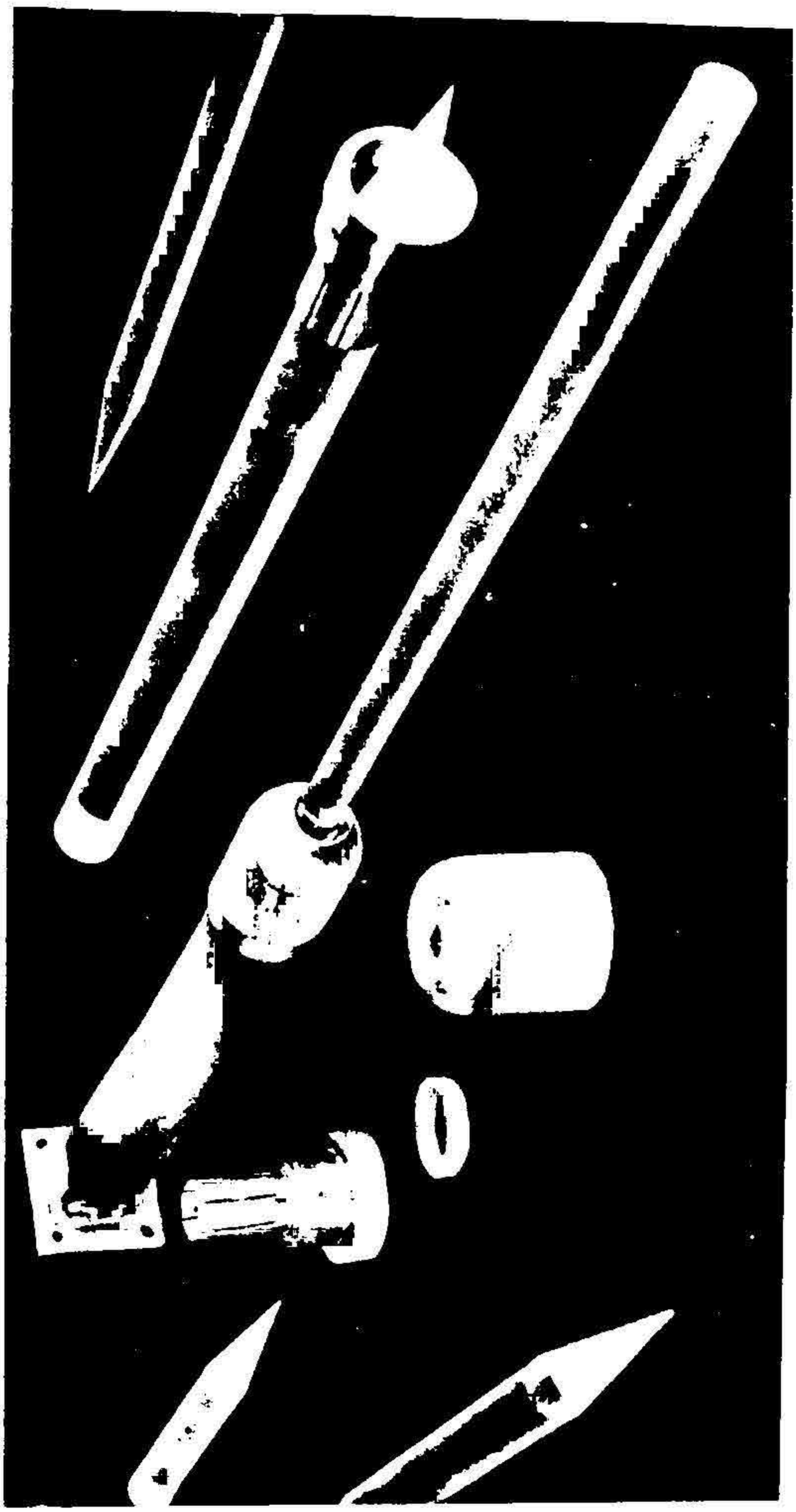

FIG. 3. Photograph of some of the dielectric aerials, split collars and waveguide transformer constructed for the experiment.

Acknowledgment

The authors acknowledge with thanks the help rendered by Messrs. Chandrasekhar and Sridhar of the Civil and Hydraulics Department in aligning the aerial stands.

References

Chatterjee, R. (Mrs.) and Chatterjee, S. K. — *Jour. Ind. Inst. Sci.*, 1956, **38**, 93.

———— .. *Ibid.*, 1957, **39**, 134.

Chatterjee, S. K. and Vasudeva Rao, B. — *Ibid.*, 1955, **37**, 304.

Chatterjee, S. K., Shenoy, P. R. and Rama Bai (Miss) — *Ibid.*, 1954, **36**, 107.